Desalination and Water Treatment
www.deswater.com

doi: 10.5004/dwt.2017.21042

81 (2017) 252–264
June

Removal of methylene blue from water using eggshell membrane fixed bed

Radia Zerdoum[a,b], Zhour Hattab[b,*], Yamina Berredjem[a], Radia Mazouz[b], Ridha Djellabi[b], Naima Filali[b], Abdelhak Gheid[a], Kamel Guerfi[b]

[a]*Science and Technology Laboratory of Water and Environment, Faculty of Science and Technology, Department of Material Sciences, University Mohammed-Cherif Messadia, Souk Ahras 41000, Algeria*
[b]*Laboratory of Water Treatment and Valorization of Industrial Wastes, Faculty of Sciences, Department of Chemistry, Badji Mokhtar University, B.P.12, Annaba 23000, Algeria, Tel. 00213 797 598 522; email: zoumourouda20012000@yahoo.fr (Z. Hattab)*

Received 23 December 2016; Accepted 16 June 2017

ABSTRACT

The purpose of this work was to remove methylene blue (MB) from water using natural eggshell membrane (ESM) in fixed-bed column. The ESM was treated and characterized by Fourier transform infrared spectra (FTIR), scanning electron microscope (SEM) and X-ray diffraction (XRD). A series of experiments were carried out to investigate the effects of bed height on breakthrough curve, flow rate, MB concentration, solution pH (2–10), the ionic strength and temperature on the adsorption behavior. The experimental results show that the adsorption capacity increases with the increase in the bed depth and MB concentration. However, it decreases with increasing the flow rate and temperature. The ESM adsorption capacity of MB is more pronounced in basic medium. The addition of NaCl salt ions decreases the fixation of MB on ESM. Five kinetic models, Bohart–Adams, Wolborska, Thomas, Yoon–Nelson and bed depth service time (BDST) models were applied to experimental data in order to predict the breakthrough curves using non-linear regression and to determine the characteristic parameters of the column useful for process design. The results showed that Thomas and Yoon–Nelson models were found suitable for the normal description of breakthrough curve at the experimental condition, while Adams–Bohart and Wolborska models were only for an initial part of dynamic behavior of the ESM column. Desorption of MB from ESM bed was performed with distilled water as the desorbing agent, and reuse study was investigated.

Keywords: Eggshell membrane; Methylene blue; Non-linear regressive; Dynamic sorption; Modeling

1. Introduction

Nowadays, the issue of water contamination has become a major issue worldwide, with the rapid development of modern industries [1]. Industrial effluents are one of the major causes of environmental pollution. Dyes are generally very toxic [2] and slightly biodegradable, which engender wastewaters with characteristic high color, high organic matter content, high chemical oxygen demand and low biochemical oxygen demand. The cationic dyes are generally utilized for various purposes because of their applicability, durability and good fastness to the materials; however, their demerit effects are immense. Cationic dyes are known to have carcinogenic, mutagenic and high coloring effects for the whole ecosystem when released as waste in the environment [3].

Methylene blue (MB), a cationic dye, has wide applications which make it one of the common dye effluents. A few endeavors have been made by scientists to address MB health effect as a pollutant in wastewater through the development and application of various adsorbents for its uptake [4–7]. Recently, many works have been investigated for the development of low-cost adsorbents for water treatment including natural biosorbents [8–10], industrial and agricultural waste materials [11–13].

Eggshell membrane material (ESM) as a low-cost absorbent, eco-friendly and abundant has been explored as a novel

* Corresponding author.

absorbent for the removal of pollutant in the fixed-bed column system from aqueous solution [14]. The eggshell membrane, which is the thin layer between the egg white and the shell, is composed of network of fibrous proteins that has a large surface area with special functional groups such as hydroxyl (–OH), sulfhydryl (–SH), carboxyl (–COOH), amino ($–NH_2$), etc, which strongly interact with several pollutant species. Because of the presence of these functions in ESM structure, it could be a successful sorbent for water treatment [15]. On the other hand, it was estimated that one eggshell membrane contains between 7,000 and 17,000 pores. Many studies [16] have been conducted to explore useful applications for eggshell membrane. Such research studies have shown that eggshell membrane is able to adsorb dyes [17] and heavy metal ions in waters and wastewaters [18]. Also, it is a biocompatible material which is easily degraded, resulting in little secondary pollution for environmental and biological safety [15].

On the other hand, recovery of MB from aqueous solution was widely studied using different techniques and materials. Several researchers have applied several low-cost materials such as jackfruit (*Artocarpus heterophyllus*) leaf powder [19], natural zeolite [20], carbon prepared from oil palm shell [3], guava (*Psidium guajava*) leaf powder [21] to remove MB from aqueous solution. However, to date, no study has ever performed using ESM as an adsorbent to remove MB in fixed bed.

The aim of the present study is to explore the possibility of utilizing ESM for adsorptive removal of MB from water using fixed-bed adsorption column. The effects of different parameters such as: bed depth, flow rate, initial MB concentration, pH, ionic strength and temperature were investigated on the adsorption capacity. Finally, five models were studied: Adams–Bohart, Wolborska, Thomas, Yoon–Nelson and BDST.

2. Materials and methods

The ESM material was obtained from the eggshell wastes collected from different local restaurants. Sodium hydroxide (NaOH), hydrogen chloride (HCl), sodium chloride (NaCl) and MB (C.I. 52015 $C_{16}H_{18}ClN_3S$) were purchased from Sigma-Aldrich-Fluka (Saint-Quentin, Fallavier, France). Solutions were prepared using distilled water. The synthetic dye solution was prepared by dissolving an accurately weighed amount of dye (1 g L^{-1}) in distilled water and subsequently diluted to the required concentration.

2.1. Preparation of ESM adsorbent

Firstly, the eggshell was washed with water and boiled in distilled water for 15 min to remove residual impurities. Then the ESM was manually stripped from eggshell and finally dried at ambient air for 24 h. The eggshell membrane was further ground to prepare powders particles. The powder was filtered and only the particles of size between 360 and 500 μm were used. The powder obtained was dried at 50°C, and then stored in desiccators until usage. The adsorption tests were carried out in dynamic mode.

2.2. ESM characterization

Sample of ESM was characterized by Fourier transform infrared analysis (FTIR), scanning electron microscope (SEM) and X-ray diffraction (XRD) methods. FTIR was recorded to identify the functional groups of ESM material using the IR Affinity –1 in combination with a single reflection ATR. Scanning electron microscope (JEOL JSM 6390 LU) model was used for determination of the ESM morphological structure before and after adsorption of MB. XRD measurements were performed on a Shimadzu XRD-6000 diffractometer using copper Kα radiation (λ = 1.5060 Å), generator setting of 40 kV, 40 mA, a scanning speed of 0.01° min^{-1} and a 2θ angle ranging from 3 to 70.

2.3. Column adsorption experiments

Column experiments were conducted at the laboratory scale in a glass column (diameter: 11 mm, length: 300 mm). Different quantities of ESM, 0.06, 0.11 and 0.165 g corresponding to 10, 20 and 30 mm bed heights, respectively, were measured using the column. Different flow rates 1, 2 and 3 mL min^{-1} were applied using a peristaltic pump (ISMATEC A39494) to adsorb MB at different initial concentrations 5, 10 and 15 mg L^{-1}.

MB solution with initial concentration flowed from the top of the column. The flow rate was controlled by a constant flow pump. The flow to the column continued until the effluent dye concentration at time t (C_t) reached the influent dye concentration (C_0): C_t/C_0 ~ 0.98. The performance of the packed bed is described in the present work using the concept of the breakthrough curve. Samples are collected at regular intervals (3 min) from the exit of the column. The residual concentration of MB was determined at a wavelength of λ_{max} = 664 nm using UV–Vis spectrophotometer (JENWAL 7315). The biosorption study was performed at room temperature 20°C ± 2°C and initial pH of 7 ± 0.2. Adjustment of the pH solution was effected with HCl (0.1 M) and NaOH (0.1 M) and monitored by a pH meter (HANNA HI9812–5). Operation of the column was stopped when the ESM adsorbent becomes saturated. The desorption of MB molecules adsorbed in the ESM bed column was carried out by washing with distilled water. The regenerated ESM bed column was reused to adsorb MB at the following conditions: flow rate: 2 mL min^{-1}, bed depth: 20 mm and MB concentration: 10 mg L^{-1}. The adsorption experiments were repeated at least twice and the average error was around 3%.

2.4. Analysis of experimental data

The MB adsorption breakthrough profiles were obtained from $\frac{C_t}{C_o}$ vs. t (min) plot; where C_t is effluent concentration, C_0 influent concentration and t is the service time. The volume of effluent treated is determined as [22]:

$$V_{\text{eff}} = Ft_e \tag{1}$$

where F (mL min^{-1}) and t_e (min) are the influent flow rate and time of exhaustion.

The total quantity of MB adsorbed in the ESM bed column (q_{total}) is calculated from the area below breakthrough curve multiplied with flow rate by using the following equation [23]:

$$q_{\text{total}} = \frac{FA}{1000} = \frac{F}{1000}\int_{t=0}^{t=\text{total}} C_{\text{ad}}\,dt \tag{2}$$

where C_{ad} equals to $(C_0 - C_t)$ and the breakthrough is obtained by plotting C_{ad} vs. time t. A is the area under C_{ad} vs. t curve, C_0 is initial MB concentration and C_t is effluent MB concentration, respectively. The uptake $q_{\text{eq(exp)}}$ (mg g^{-1}) is calculated by dividing q_{total} to the biosorbent mass (m) [24]:

$$q_{\text{eq(exp)}} = \frac{q_{\text{total}}}{m} \tag{3}$$

From the adsorption capacity, N_{exp} (mg L^{-1}) can be calculated by the following equation:

$$N_{\text{exp}} = q_{\text{exp}}\frac{m}{V} \tag{4}$$

where V (mL) is the volume of the adsorbent.

Amounts of adsorbate passed into the column W_{total} (mg) is determined as follows:

$$W_{\text{total}} = \frac{C_0 Q t_{\text{total}}}{1000} \tag{5}$$

The percentage adsorbate uptake is calculated as follows:

$$R\% = \frac{q_{\text{total}}}{W_{\text{total}}} \times 100 \tag{6}$$

2.5. Kinetic models of ESM fixed-bed column adsorption

In this study, five theoretical models, Bohart–Adams, Wolborska, Thomas, Yoon–Nelson and BDST have been applied to predict the breakthrough curves.

2.5.1. Bohart–Adams model

The Bohart–Adams model was used for the description of the initial part of the breakthrough curve. This model assumes that the adsorption rate is proportional to the residual capacity of the solid and the concentration of the adsorbed substance [25]. The model equation can be expressed as follows [26]:

$$\frac{C_t}{C_0} = \exp\left(K_{\text{BA}} C_0 t - K_{\text{BA}} N_0 \frac{Z}{U}\right) \tag{7}$$

where C_0 and C_t (mg L^{-1}) are the initial and breakthrough concentrations, K_{BA} (L mg^{-1} min^{-1}) is the sorption rate coefficient, N_0 (mg L^{-1}) is the fixed-bed sorption capacity per unit volume, Z (mm) is the bed depth in the column, U (mm min^{-1}) is the linear velocity and t (min) is the time.

2.5.2. Wolborska model

Wolborska [27] has proposed a model based on the general equations of mass transfer for diffusion mechanism in the range of the low concentration breakthrough curve. The Wolborska sorption model was applied to experimental on data for the description of the initial part of the breakthrough curve which can be defined as:

$$\frac{C_t}{C_0} = \exp\left(\frac{\beta_a C_0}{N_0} t - \frac{\beta_a Z}{U}\right) \tag{8}$$

The parameters of the Wolborska equation are β_a (min^{-1}), representing the kinetic coefficient of the external mass transfer, and N_0 (mg L^{-1}), representing the saturation concentration of the fixed-bed reactor.

2.5.3. Thomas model

This model has been applied for biosorption progress where the external and internal diffusion limitations are absent [28]. The Thomas model is used to calculate the adsorption rate constant and the solid phase concentration of the dye on the adsorbent from the continuous mode studies. The model has the following form:

$$\frac{C_t}{C_0} = \frac{1}{1 + \exp\left(\frac{K_{\text{th}} q_{\text{th}} m}{Q} - k_{\text{th}} C_0 t\right)} \tag{9}$$

The kinetic coefficient K_{th} and the adsorption capacity of the column q_{th} can be determined from a plot of $\frac{C_t}{C_o}$ against t for a given flow rate using non-linear regression analysis.

2.5.4. Yoon and Nelson model

Yoon and Nelson [29] developed a relatively simple model for the adsorption and breakthrough of adsorbate vapors or gases onto activated charcoal. The model is based on the assumption that the rate of decrease in the probability of adsorbate molecule is proportional to the probability of adsorbate breakthrough on the adsorbent.

The Yoon and Nelson model is not only less complicated than other models, but also requires no detailed data concerning the characteristics of adsorbate, the type of adsorbent and the physical properties of adsorption bed. For a single-component system, it can be expressed as follows [29]:

$$\frac{C_t}{C_0 - C_t} = \exp(K_{\text{YN}} t - \tau K_{\text{YN}}) \tag{10}$$

where K_{YN} is the rate constant (min^{-1}), τ is the time required for 50% sorbate breakthrough (min) and t is the time (min). The parameters of K_{YN} and τ can be obtained using the non-linear regressive method.

2.5.5. Bed depth service time analysis model

The bed service time model was proposed by Bohart and Adams in 1920 in their study on the adsorption of chlorine in charcoal [26]. The model is based on the assumption that the rate of adsorption is controlled by the surface reaction between adsorbate and the unused capacity of the adsorbent [30]. The bed depth service time model can be used to

estimate the required bed depth for a given service time. A linear relationship between and bed depth and service time is given by the following Eq. (11) [30]:

$$t_b = \frac{N_0'}{C_0 U} Z - \frac{1}{K_{BA} C_0} \ln\left(\frac{C_0}{C_b} - 1\right) \quad (11)$$

where t_b (min) is the service time and C_b (mg L^{-1}) is the specific breakthrough concentration. $N_0'(mg.L^{-1})$ is the sorption capacity, C_0 (mg L^{-1}) is the initial concentration, U (mm min^{-1}) is superficial fluid velocity and Z (mm) the height of the fixed bed.

2.6. Test of kinetic models

The parameters of different kinetic models were obtained using non-linear analysis according to the least normalized standard deviation, SD (%) and chi-square test x^2. The conformity of model is better when the correlation coefficient is higher [31] and the error is lower [32]. The relative mathematical formulas are:

$$x^2 = \sum_{i=1}^{n} \frac{\left[\left(\frac{C_t}{C_0}\right)_c - \left(\frac{C_t}{C_0}\right)_e\right]^2}{\left(\frac{C_t}{C_0}\right)_c} \quad (12)$$

$$SD = 100 \times \left\{ \sum \frac{\left[\left(\left(\frac{C_t}{C_0}\right)_c - \left(\frac{C_t}{C_0}\right)_{exp}\right) / \left(\frac{C_t}{C_0}\right)_{exp}\right]^2}{N-1} \right\}^{1/2} \quad (13)$$

where $(c_t/c_0)_c$ is the ratio of effluent and influent MB concentrations obtained from calculation according to dynamic models, and the $(c_t/c_0)_e$ is the ratio of effluent and influent MB concentrations obtained from experiment, respectively, and N is the number of experimental data.

3. Results and discussion

3.1. Characterization of ESM

3.1.1. SEM analysis

The morphological structure of ESM before adsorption presented in Fig. 1(a) revealed by SEM analysis showed that ESM appears as rod-like fibrous fractures [33]. However, after the adsorption of MB (Fig. 1(b)), there is porosity loss of ESM surface resulting from the accumulation of MB molecules.

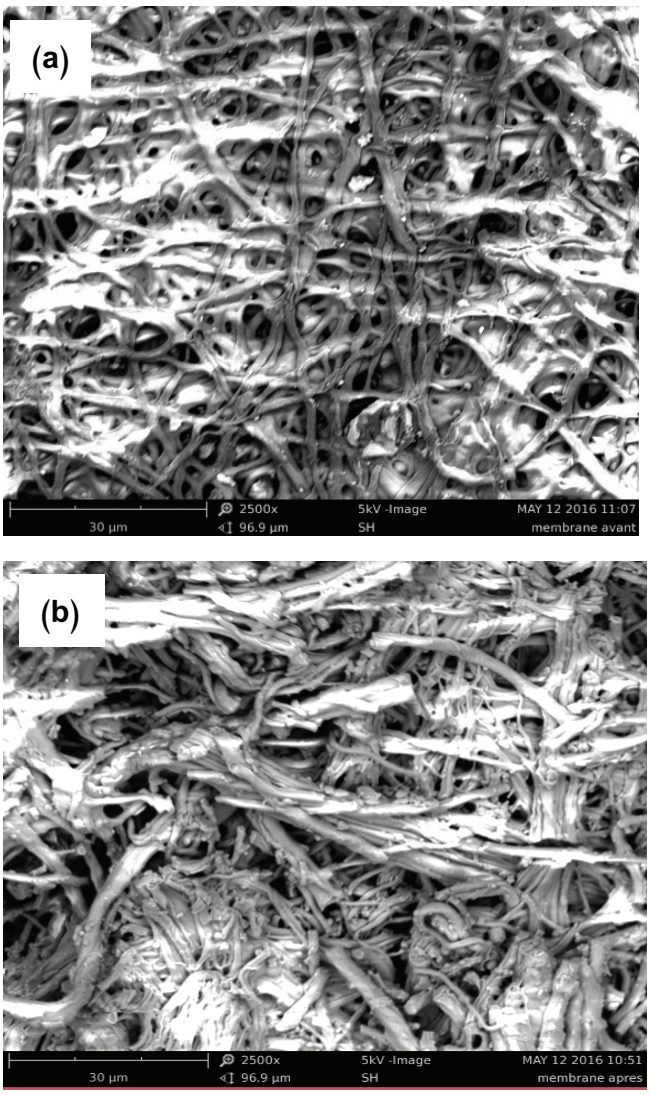

Fig. 1. SEM photographs (X 2500) of (a) eggshell membrane before MB adsorption and (b) eggshell membrane after MB adsorption.

3.1.2. Fourier transform infrared spectroscopy analysis

FTIR spectra of ESM before and after MB adsorption are shown in Fig. 2. FTIR spectrum can be divided into two regions: the first one is between 3,725 and 2,300 cm^{-1}, and the second one is below 1,700 cm^{-1}. In the first region, the most

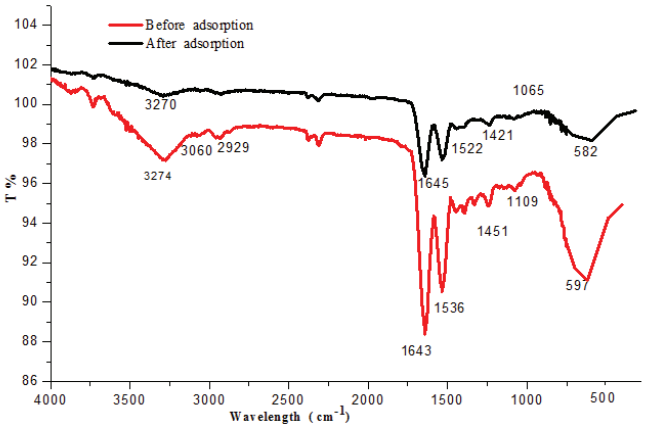

Fig. 2. FTIR spectra of ESM before and after adsorption of MB.

intense peak is fixed at 3,274 cm^{-1}, which corresponds to the stretching mode of O–H and N–H groups. Peaks at 3,060 and 2,929 cm^{-1} correspond to the asymmetric stretching vibrations of the C–H bonds present in =C–H and $=CH_2$ groups [34]. However, in the second region, peaks correspond to the following groups: at 1,643 cm^{-1}: amide C=O stretching, 1,536 cm^{-1}: vibration amide N–H bending, 1,451 cm^{-1}: CH_2 scissoring, 1,109 cm^{-1}: C–N stretching and 597 cm^{-1}: C–S [35–37]. On the other hand, after MB adsorption, it is observed that the intensity of the following peaks: OH and N–H: 3,270 cm^{-1}, C=O: 1,522 cm^{-1}, amide N–H: 1,421 cm^{-1}, amine C–N: 1,065 cm^{-1} decreased. These shifts indicate that the interaction was occurred between MB functional groups and ESM surface.

3.1.3. X-ray diffraction

X-ray diffractogram of ESM is presented in Fig. 3. XRD analysis is very important to distinguish which kind of the material structure is and to identify the crystal composition. From the XRD pattern, we notice that the material does not have any kind of crystal structure (there are no diffraction peaks) which confirms that this material has no crystal structure (amorphous).

3.2. Effect of flow rate on the breakthrough curve

To investigate the effect of flow rate on MB adsorption, different flow rates varies from 1.0 to 3.0 mL min^{-1} were tested at MB concentration of 10 mg L^{-1} and ESM bed depth equal to 20 mm. The breakthrough curves of MB adsorption at different flow rates are illustrated in Fig. 4. From these results, we can notice that the breakthrough generally occurred faster with a higher flow rate. The break point of the curve reaching saturation was significantly increased with a decrease in flow rate. The results are summarized in Table 1. An increment in the flow rate from 1.0 to 3.0 mL min^{-1} leads to the MB adsorption speed. The increase of the flow rate affects the mass transfer (diffusion of MB molecules to the ESM porous). Therefore, a quick reaction between MB molecules and ESM functional groups takes place.

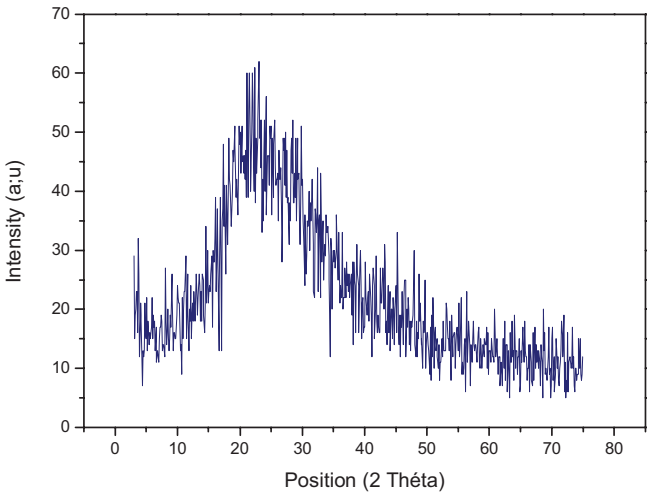

Fig. 3. XRD analysis results for the ESM before adsorption.

3.3. Effect of bed depth (amount of adsorbent) on the breakthrough curve

The breakthrough curves at different ESM bed depths (10, 20 and 30 mm) and at MB concentration of 10 mg L^{-1} and flow rate equal to 2.0 mL min^{-1}, were plotted. The results obtained are shown in Fig. 5 and summarized in Table 1. The MB adsorption was significantly enhanced with the increment of ESM bed depth. A higher bed depth contains more adsorption sites and higher surface area, resulting in a faster adsorption of MB molecules [3]. However, in the shorter bed, the exhaustion approached faster and performance declined. Similar results have been obtained in other studies [38, 39].

3.4. Effect of initial concentration on the breakthrough curve

To evaluate the effect of initial MB concentration on the breakthrough curve, a set of adsorption experiments was performed using 20 mm of sorbent bed depth, 2 mL min^{-1} of feed flow rate and varying the MB inlet concentration (5–15 mg L^{-1}). The results shown in Fig. 6 demonstrated that the increase of the initial MB concentration led to a decrease of the breakthrough time. At the first 66 min of the column operation, the value of c_t/c_0 reached 0.02, 0.015 and 0.01 when the inlet concentrations were 15, 10 and 5 mg L^{-1}, respectively. The extension of breakthrough point in the lower influent concentration was due to lower mass transfer in the adsorption process which leads to the treatment of more volume of MB solution [40]. The results indicate that the adsorbent is capable of holding a maximum adsorption capacity of 28.745 mg g^{-1} at 15 mg L^{-1} of influent concentration.

Total adsorbed MB quantity (q_{total}), removal percentage and the experimental adsorption capacity increased with MB inlet concentration from 5 to 15 mg L^{-1}.

4. Modeling

4.1. Bohart and Adams model

The model's experimental sorption capacity N_0 was found to increase with the increase in MB concentration. It decreases

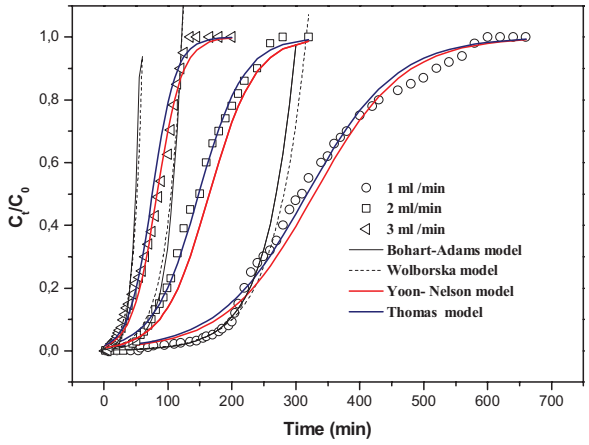

Fig. 4. Comparison of the experimental and predict breakthrough curves obtained at different flow rates according to the studied models for methylene blue adsorption by ESM (pH = 7 ± 0.2, C_0 = 10 mg L^{-1} and Z = 20 mm).

Table 1
The conditions and the results for the fixed-column experiments (T = 20 ± 2°C, pH = 7 ± 0.2)

C_0 (mg L^{-1})	Z (mm)	F (mL min^{-1})	t_b (min)	t_{total} (min)	V_{eff} (mL)	W_{total} (mg)	q_{total} (mg)	q_{exp} (mg g^{-1})	R (%)
10	10	2	15	160	320	3.2	1.6	26.611	50.00
10	20	2	39	280	560	5.2	2.9	27.910	55.77
10	30	2	70	500	1,000	9.2	4.7	29.260	51.11
5	20	2	66	360	720	3.6	1.83	16.636	50.83
15	20	2	21	180	360	5.1	3.16	28.745	61.96
10	20	1	66	600	600	5.6	3.248	30.937	58.00
10	20	3	10	145	435	4.35	2.12	19.272	48.73

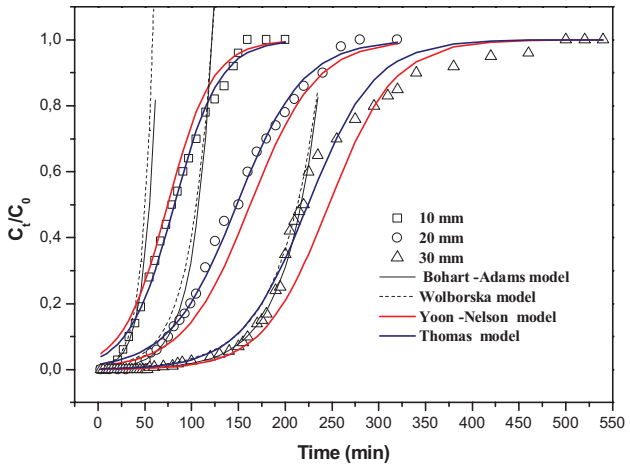

Fig. 5. Comparison of the experimental and predict breakthrough curves obtained at different ESM bed heights according to the studied models for methylene blue adsorption by ESM (pH = 7 ± 0.2, C_0 = 10 mg L^{-1} and D = 2 mL min^{-1}).

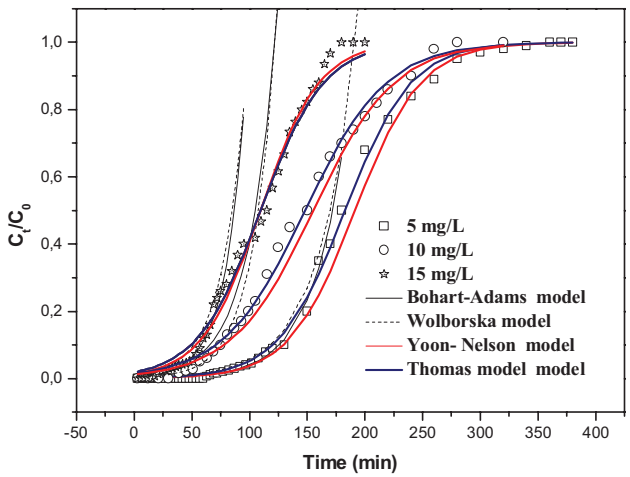

Fig. 6. Comparison of the experimental and predict breakthrough curves obtained at different MB concentrations according to the studied models for methylene blue adsorption by ESM (pH = 7 ± 0.2, Z = 20 mm, F = 2 mL min^{-1}).

with the increment in solution flow rate for adsorption of MB on ESM (Table 2). Also, it is observed that the mass transfer coeffecient, K_{BA}, decreases with a rise in the initial MB concentration. This is attributed to dominance of external mass transfer activities during adsorption in the column at the initial stages [41]. The model well predicted the breakthrough time, especially at higher bed height.

4.2. Wolborska model

N_0 and β_a were calculated from C_t/C_o vs. t (min) plot for all concentrations, flow rate and bed height are presented in Table 2. According to the values, it was observed that K_{BA} is equal to β_a/N_o which indicated that the expression of Wolborska solution is equivalent to the Adams–Bohart relation. The values of β_a are decreased while N_0 increased. It was concluded that overall system kinitics is dominated by the external mass transfer in the initial part of dynamic biosorption.

4.3. Thomas model

From Table 2 it is seen that the Thomas rate constant decreases with an increase in influent dye concentration. The reason is that the driving force for adsorption is the concentration difference between the dye on the adsorbent and the dye in the solution [42]. However, as the bed heights increased the value of q_{th} increased, but the value of K_{th} decreased. With flow rate increasing, the values of q_{th} decreased and the value of K_{th} increased. It is noticed that values of determined coefficients are higher (R^2 > 0.98). It is also interestingly observed from the data summarized in Table 2 that the q_{th} values calculated from the Thomas model are very close to the amount value obtained experimentally, termed as q_{exp}. It can be argued that the Thomas model is the most suitable one to describe MB adsorption in the ESM fixed bed.

4.4. Yoon and Nelson model

The fitting results are tabulated in Table 2, and they show that the rate constant K_{YN} increased and τ decreased with increasing flow rate. This was due to the fact that higher flow rate would result in the insufficiancy of the adsorption and achieving the adsorption equilibrium early. However, the same trend was also observed when the bed heights increased the rate constant K_{YN} decreased. The data in Table 2 also indicate that values of τ are similar to the experimental results, the R^2 are superior to 0.98 and x^2 less than 0.00150, which indicates that the data fits into the model perfectly [43]. Han et al. [44] reported that the values of K_{YN} and τ correspond well to experimental data. The same conclusion was found by Aksu and Gonen [42].

Table 2
Parameters of various models for MB adsorption by ESM at different conditions using non-linear regression. Experimental fixed conditions: $T = 20 \pm 2°C$, pH = 7 ± 0.2

Z (mm)	C_0 (mg L^{-1})	U (mL min^{-1})	Adams–Bohart model (up to 15%)						Wolborska model (up to 15%)					
			$K_{BA} \times 10^3$ (mL mg^{-1} min^{-1})	N_0 (mg L^{-1})	N_{exp} (mg g^{-1})	R^2	$x^2 \times 10^3$	SD (%)	B_a (min^{-1})	N_0 (mg L^{-1})	N_{exp} (mg L^{-1})	R^2	$x^2 \times 10^3$	SD (%)
10	10	2	8.12 ± 1.02	1,336.60 ± 74.31	1,234.96	0.96085	0.128	1.13	10.86 ± 0.79	1,336.40 ± 74.15	1,234.96	0.96090	0.128	1.13
20	10	2	4.88 ± 0.31	1,285.92 ± 33.60	1,300.12	0.98328	0.035	0.60	6.24 ± 0.24	1,356.66 ± 36.30	1,300.12	0.97966	0.059	0.77
30	10	2	2.79 ± 0.09	1,708.28 ± 18.93	1,362.96	0.99102	0.015	0.39	4.70 ± 0.10	1,708.25 ± 18.91	1,362.95	0.99102	0.014	0.39
20	5	2	1.04 ± 0.02	1,010.96 ± 22.69	774.94	0.95611	0.035	0.59	7.03 ± 0.23	1,011.14 ± 22.64	897.72	0.95619	0.035	0.59
20	15	2	2.20 ± 0.14	1,571.10 ± 40.74	1,339.01	0.97079	0.847	0.84	5.85 ± 0.19	1,571.05 ± 40.68	1,441.11	0.97079	0.044	0.66
20	10	1	3.73 ± 0.02	1,583.87 ± 36.16	1,441.11	0.97580	0.046	0.69	3.49 ± 0.14	1,588.48 ± 35.23	1,339.01	0.97653	0.043	0.62
20	10	3	6.96 ± 0.38	750.92 ± 70.70	897.72	0.94009	0.121	1.10	7.83 ± 0.70	750.84 ± 70.43	774.94	0.94009	0.121	1.10
Z (mm)	C_0 (mg L^{-1})	U (mL min^{-1})	Thomas model						Yoon and Nelson model					
			$K_{th} \times 10^3$ (mL mg^{-1} min^{-1})	q_{th} (mg g^{-1})	q_{exp} (mg g^{-1})	R^2	$x^2 \times 10^3$	SD (%)	$K_{YN} \times 10^3$ (mL min^{-1})	τ (min)	τ_{exp} (min)	R^2	$x^2 \times 10^3$	SD (%)
10	10	2	4.16 ± 0.16	27.17 ± 0.32	26.61	0.99327	0.924	3.08	41.56 ± 1.60	81.51 ± 0.97	79	0.99193	0.947	3.20
20	10	2	2.84 ± 0.76	29.66 ± 0.29	27.91	0.99539	0.600	2.45	28.30 ± 0.76	158.53 ± 1.13	149	0.98919	0.612	2.55
30	10	2	2.81 ± 0.13	32.62 ± 0.20	29.26	0.98711	1.450	3.80	28.20 ± 0.13	246.29 ± 1.75	211	0.97444	1.500	4.02
20	5	2	7.48 ± 0.16	16.63 ± 0.07	16.63	0.99817	0.270	1.64	35.20 ± 0.86	190.85 ± 0.85	182	0.99775	0.282	1.68
20	15	2	2.62 ± 0.73	29.90 ± 0.24	28.74	0.99142	0.976	3.13	39.30 ± 1.13	109.64 ± 0.87	114	0.99133	0.979	3.45
20	10	1	1.44 ± 0.46	30.25 ± 0.22	30.94	0.99218	1.110	2.98	14.40 ± 0.46	338.22 ± 2.39	311	0.98071	1.330	3.33
20	10	3	5.49 ± 0.31	20.80 ± 0.32	19.27	0.99088	0.700	3.92	54.90 ± 3.12	75.59 ± 1.20	76	0.99120	0.666	3.92

4.5. Bed depth service time

Fig. 7 shows that the plots of the service time (t_b) at 10%, 30%, 60% and 90% breakthrough points, that is, t_b at C_t/C_0 equal to 0.1, 0.3, 0.6 and 0.9, respectively, vs. the bed height and the BDST constants listed in Table 3. All the coefficients of determination R^2 exceeded 0.98, indicating that the BDST model might be applicable to represent the MB adsorption in ESM fixed-bed column. At C_b/C_0 around 0.6 and 0.9, the simulated K_{BA} were abnormal and showed negative values, which might be due to the limitation of BDST model. The results found are in agreement with other studies [45].

5. Effect of initial solution pH on the breakthrough curve

The pH factor is very important in the adsorption process, especially, for dye adsorption. The results of the pH effect on the breakthrough curves are shown in Fig. 8. The calculated results are listed in Table 4 and the experimental data were fitted by Thomas model. At pH 8–10, ESM reached the highest MB adsorption capacity of 38.460 and 70.214 mg g^{-1}, respectively. However, at pH 6–2 the adsorption capacity decreases from 18.612 to 0.818 mg g^{-1}. ESM contains positively charged functional groups as $–NH_3^+$ and $–CO–NH_2^+$ which are dependent on the pH of the aqueous solution [46], that is, when the initial pH was lower than 6.0, the ESM acquires the positive charge, the predominant species of MB will compete with the high concentration of H^+ to bind to the active sites of adsorbent, the adsorption equilibrium was achieved rapidly and a few MB could be adsorbed onto ESM. However, at the initial pH higher than 6.0, few carboxyl groups were protonized, the electrostatic interaction between the ESM and cationic MB become significantly attractive, and hence resulted in the increase of MB uptake.

6. Desorption and column regeneration

Regeneration of spent adsorbent is one of the important economic factors in assessing the feasibility of an adsorption system. Fig. 9 shows the desorbed curves. Fig. 10 shows the recycles of biosorbed MB by ESM. After column adsorption, the regeneration of ESM fixed bed was carried for three cycles. The simulated results by Thomas model were summarized in Table 5. The values of elution efficiency were 49.79%, 33.97% and 19% for the three respective biosorption elusion cycles. Similar percentages have been reported for desorption of MB using distilled water [47]. It is important to note that the third regeneration cycle took 125 min, after which further MB desorption was negligible.

7. Effect of ionic strength

In this study, the effect of the ionic strength on the adsorption of MB on ESM fixed bed was investigated at two NaCl concentrations (0.1 and 0.01 N). The breakthrough curves are showed in Fig. 11. It is observed that with an increase of ionic strength from 0.01 to 0.1 mg L^{-1}, the MB adsorption capacity decreases from 17.090 to 5.954 mg g^{-1}. This is due the Na^+ ions which are positioned adjacent to the surface of ESM. The association of positive ions around the adsorbent causes a decrease

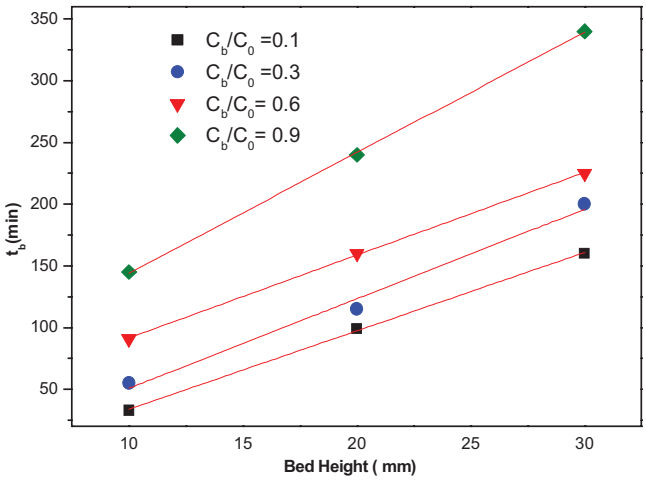

Fig. 7. Linear regression of the BDST model at different breakthrough points (C_0 = 10 mg L^{-1} and Q = 2 mL min^{-1}).

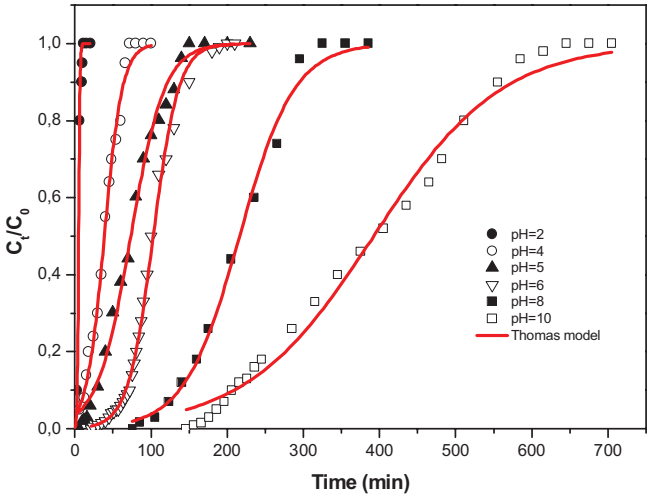

Fig. 8. Effect of pH solution on the breakthrough curves (Z = 20 mm, C_0 = 10 mg L^{-1} and Q = 2 mL min^{-1}).

Table 3
Calculated constants of the BDST model for adsorption of MB (C_0 = 10 mg $L^{-1}$and Q = 2 mL L^{-1})

C_b/C_0	a (min mm^{-1})	b (min)	$K_{AB} \times 10^3$ (L mg^{-1} min^{-1})	N_0' (mg L^{-1})	R^2
0.1	6.35 ± 0.14	29.666 ± 3.11	7.405	1,336.9925	0.9989
0.3	7.25 ± 0.72	21.666 ± 15.59	3.910	1,526.4857	0.9804
0.6	6.70 ± 0.11	24.666 ± 2.49	–1.643	1,410.6850	0.9994
0.9	9.75 ± 0.14	46.666 ± 3.11	–4.710	2,052.8625	0.9904

Table 4
Thomas parameters for MB adsorption by ESM in fixed-bed systems at various pH

pH	Z (mm)	C_0 (mg L^{-1})	Q (mL min^{-1})	$K_{th} \times 10^3$ (mL mg^{-1} min)	q_{th} (mg g^{-1})	q_{exp} (mg g^{-1})	R^2	$x^2 \times 10^3$	SD (%)
2	20	10	2	113.70 ±16.67	0.880 ± 0.03	0.818	0.99123	1.80	4.24
4	20	10	2	8.50 ± 0.40	6.960 ± 0.11	6.520	0.99282	1.08	3.29
5	20	10	2	4.53 ± 0.20	13.351 ± 0.20	12.950	0.99287	1.01	3.17
6	20	10	2	6.05 ± 0.18	18.715 ± 0.11	18.719	0.99649	0.50	2.25
8	20	10	2	2.77 ± 0.10	39.274 ± 0.30	38.460	0.99375	0.48	2.20
10	20	10	2	1.19 ± 0.05	71.350 ± 0.81	70.214	0.98920	1.45	3.8

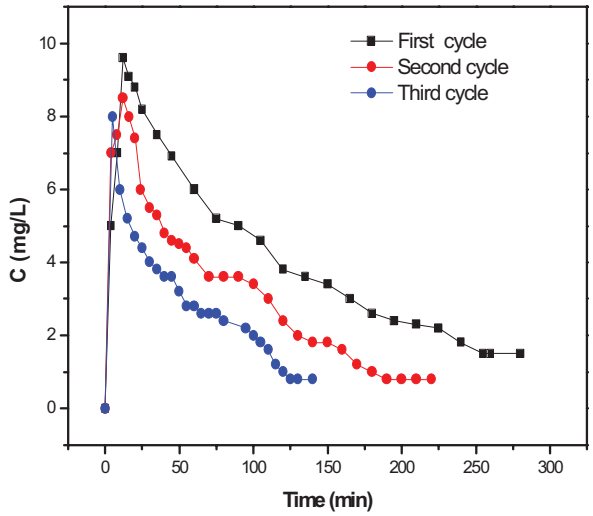

Fig. 9. Desorption of MB from ESM column using distilled water (F = 2 mL min^{-1}, Z = 20 mm, C_0 = 10 mg L^{-1} and T = 20 ± 2°C).

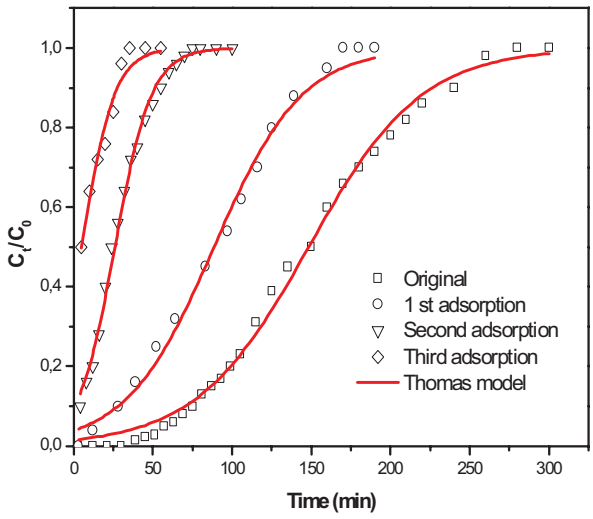

Fig. 10. Breakthrough curves for regenerated ESM (F = 2 mL min^{-1}, Z = 20 mm, C_0 = 10 mg L^{-1} and T = 20 ± 2°C).

in the contact between the MB and the active sites on ESM which leads to decrease in the adsorption process. On the other hand, Na^+ at high concentration can compete with MB molecules for the adsorption sites resulting surface saturation. Similar observation was found by other researchers [48].

8. Effect of temperature on breakthrough curves

The temperature effects have been investigated. The breakthrough curves at various temperatures and different bed heights were shown in Fig. 12. The simulated results of Thomas model were tabulated in Table 6. It has been observed that with the increase of temperature, the adsorption capacity of MB decreased, and the rate constant increased. At the same bed height, the capacity of adsorption shows clear changeable. The decrease in capacity of adsorption with rise in temperature is due to desorption caused by an increase in the available thermal energy. This phenomenon suggests that the surface is exothermic in nature and so low temperatures favor the adsorption process [49]. This result was also in accordance with that in studies batch. On the other hand, the effect of temperature was studied by Baláz [16]. It was seen that the thermal stability of ESM is not very high, because it contains proteinaceous fibers. Also, around 55°C, the thermal decomposition of ESM starts very early and the thermal denaturation of collagen takes place [50].

9. Thermodynamic analysis

The values of thermodynamic parameters, that is, free energy ($\Delta G°$), enthalpy ($\Delta H°$) and entropy changes ($\Delta S°$) of the adsorption process were investigated in batch mode by agitation of 0.2 g the adsorbent in 200 mL solution (60 mg/L of MB) and shaken at 50 rpm at different temperatures 20°C, 30°C and 40°C. The parameters of the process can be determined from the following equations:

$$\Delta G° = -RT \ln K_L \tag{14}$$

$$\ln K_L = \frac{\Delta S^\circ}{R} - \frac{\Delta H^\circ}{RT} \tag{15}$$

$$K_L = \frac{q_e}{C_e} \tag{16}$$

where K_L (L mol^{-1}) is the apparent equilibrium constant, R (J mol^{-1} K^{-1}) is the ideal gas constant and T is the absolute temperature (K).

The linear plot of $\ln K_L$ against $1/T$ gives the enthalpy change as the slope and change in entropy as the intercept as presented in Fig. 13. The thermodynamic parameters are regrouped in Table 7.

From the results, it can be deduced that $\Delta G°$ values are negative for all the temperatures, which indicate the spontaneous nature of the adsorption process. The $\Delta G°$ values in the range from –20 to 0 kJ moL^{-1} are typically to those of the physisorption process [51]. The negative values of ΔH indicated the exothermic nature of adsorption, which explain the decrease of MB efficiency as the temperature increased. Finally, the negative value of $\Delta S°$ suggests that the system exhibits random behavior. Similar results of adsorption of dyes onto different adsorbents with a negative change in entropy and enthalpy have been reported [52–55].

10. Evaluation of ESM as adsorbent

The adsorption capacity of ESM was compared with various natural adsorbents and also with a ESM/batch system for the removal of methylene blue. The comparison demonstrates that this material has an acceptable/high adsorption potential. On the other hand, from Table 8, we can notice that the adsorption capacity of ESM/fixed-bed system (our study) is more important that ESM/batch system.

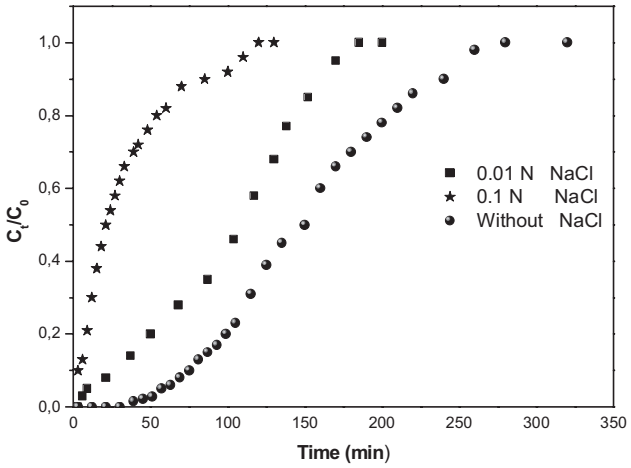

Fig. 11. The effect of the ionic strength on the adsorption capacity (C_0 = 10 mg L^{-1}, H = 20 mm, F = 2 mL min^{-1} and pH = 7 ± 0.2).

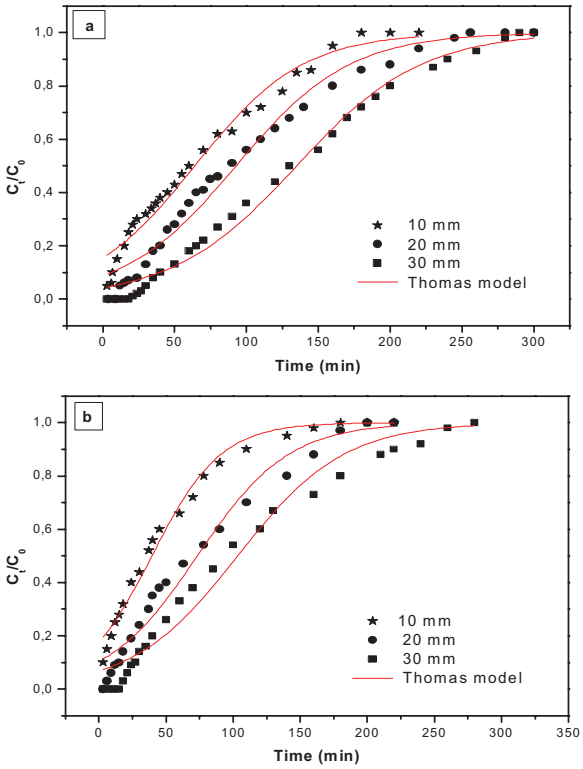

Fig. 12. Effect of bed height on the breakthrough curves at different temperatures 303 K (a) and 313 (b) (C_0 = 10 mg L^{-1}, Z = 20 mm, F = 2 mL min^{-1} and pH = 7 ± 0.2).

Table 5
Parameters of Thomas model for the biosorption of MB by ESM

	K_{th} × 10^3 (mL mg^{-1} min^{-1})	N_0 (mg g^{-1})	R^2	x^2 × 10^3	SD (%)
Original	2.84 ± 0.76	29.66 ± 0.20	0.99539	0.60	2.45
1st biosorption	3.62 ± 0.17	16.11 ± 0.25	0.99242	0.95	3.09
2nd biosorption	8.65 ± 0.27	4.71 ± 0.06	0.99515	0.45	2.12
3rd biosorption	9.74 ± 1.10	0.93 ± 0.20	0.98451	1.29	3.59

Table 6
Thomas parameters for MB adsorption by ESM in fixed bed

T (K)	Z (mm)	K_{th} × 10^3 (mL mg^{-1} min^{-1})	q_{th} (mg g–^{1})	q_{exp} (mg g^{-1})	R^2	x^2 × 10^3	SD (%)
293	10	4.16 ± 0.16	27.17 ± 0.32	26.61	0.99327	0.92	3.08
	20	2.84 ± 0.76	29.66 ± 0.29	27.91	0.99539	0.60	2.45
	30	2.81 ± 0.13	32.62 ± 0.20	29.26	0.98711	1.45	3.80
303	10	2.66 ± 0.14	21.376 ± 0.64	22.13	0.97577	2.27	4.76
	20	2.53 ± 0.14	16.876 ± 0.41	17.55	0.97828	2.47	4.96
	30	2.32 ± 0.09	16.358 ± 0.52	16.16	0.98927	1.44	3.79
313	10	3.89 ± 0.23	13.314 ± 0.45	14.76	0.98380	1.66	4.06
	20	2.94 ± 0.23	13.129 ± 0.55	13.85	0.97218	3.37	5.80
	30	2.53 ± 0.18	12.525 ± 0.45	12.91	0.97254	3.75	6.12

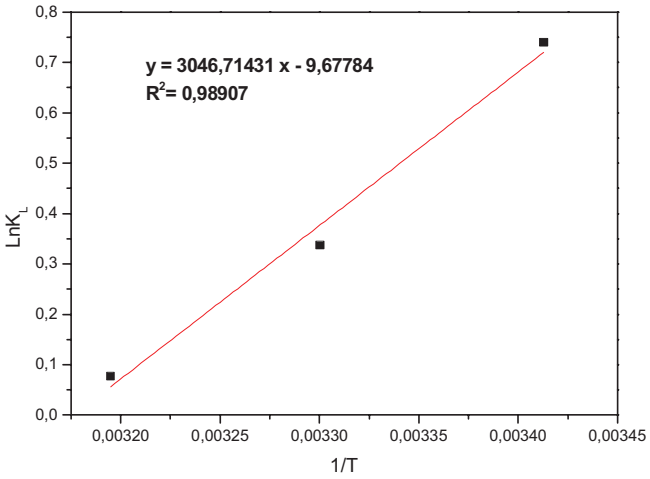

Fig. 13. Graphical determination of $\Delta H°$ and $\Delta S°$.

Table 7
Thermodynamic parameters for the adsorption of MB onto ESM

T (K)	$\Delta H°$ (kJ mol^{-1})	$\Delta G°$ (kJ mol^{-1})	$\Delta S°$ (J mol^{-1} K^{-1})
293	–25.412	–1.837	–80.461
303		–1.041	
313		–0.230	

Table 8
Comparison of adsorption capacity of various adsorbents for MB

Materials	q_m (mg g^{-1})	Reference
Granulated slag	0.29	[43]
Natural zeolite	4.47	[20]
Phoenix tree leaf	152	[44]
Guava leaf powder (*Psidium guajava*)	133.62	[21]
Olive pomace, charcoal	42.3, 62.7	[56]
ESM (batch)	4.66	[57]
ESM	70.214	This study

11. Conclusions

This study was carried out to investigate the use of fixed-bed adsorption column for the removal MB from aqueous solution using a low-cost adsorbent based on natural biomaterial eggshell membrane. The sorption of MB was dependent on the flow rate, pH, bed height and initial dye concentration. The results of this work show that the increase of bed height (adsorbent mass) led to improve the sorption performance. The ESM bed capacity was found to decrease with the increase in flow rate and temperature. The thermodynamic parameters revealed that the adsorption was spontaneous and exothermic. The increase in initial dye concentration resulted in higher uptake. A maximum uptake of 70.214 mg g^{-1} for MB adsorption by ESM, was found at 2 mL min^{-1} flow rate, 10 mg L^{-1} initial dye concentration, 20 mm bed height and pH 10. The adsorption capacity in column increases with initial solution pH reaches 10. The MB removal efficiency decreases as ionic strength increases from 0.01 to 0.1 N. Several models were applied to experimental data obtained from dynamic studies performed on fixed columns to predict the breakthrough curves and to determine the column kinetic parameters. The dynamic behavior of the column was predicted by Bohart–Adams, Wolborska, Thomas, Yoon–Nelson and BDST. All models were found suitable for describing the whole or a definite part of the dynamic behavior of the column.

Acknowledgments

The authors acknowledge the financial support of the Ministry of Higher Education of Algeria. Dr. Radia Zerdoum would like to thank people of the Laboratory of Water Treatment and Valorization of Industrial Wastes (Annaba University, Algeria) for their invaluable contributions to this work and useful discussions.

Symbols

C_0 – Initial MB concentration, mg L^{-1}
C_t – Effluent MB concentration, mg L^{-1}
V_{eff} – Effluent volume, mL
F – Influent flow rate, mL min^{-1}
q_{total} – Total weight of MB adsorbed by adsorbent in column, mg
C_{ad} – Adsorbed MB concentration, mg L^{-1}
m – Adsorbent mass, g
R – Percentage of removal, %
t_e – Time of exhaustion, min
t – Service time of the column, min
Q – Flow rate, mL min^{-1}
q_{exp} – Weight of MB adsorbed per gram of adsorbent from experiment, mg g^{-1}
N_{exp} – Experimental maximum sorption capacity, mg L^{-1}
V – Volume of solution, mL
W_{total} – Total amount of MB sent to column, mg
K_{BA} – Kinetic constant of Bohart–Adams model, L mg^{-1} min^{-1}
Z – Height of the bed, mm
N_0 – Maximum sorption capacity, mg L^{-1}
U – Linear velocity, mm min^{-1}
K_{th} – Kinetic constant of Thomas model, L mg^{-1} min^{-1}
K_{YN} – Kinetic constant of Yoon–Nelson model, min^{-1}
t_b – Time at breakthrough, min
N'_0 – Adsorption capacity in BDST model, mg L^{-1}
C_b – Breakthrough concentration, mg L^{-1}
C_e – Concentration of MB solution at equilibrium, mg L^{-1}
q_e – Amount of MB adsorbed at equilibrium, mg L^{-1}
K_L – Apparent equilibrium constant, L mol^{-1}
$\Delta G°$ – Standard free energy, kJ mol^{-1}
$\Delta S°$ – Standard entropy change, J mol^{-1} K^{-1}
$\Delta H°$ – Standard enthalpy change, kJ mol^{-1}
T – Temperature, °C, K

Greeks

β_a – Kinetic coefficient of the external mass transfer in the Wolborska model, min^{-1}
τ – Time required for 50% adsorbate breakthrough from Yoon–Nelson model, min

References

[1] S.C. Doney, The growing human footprint on coastal and open-ocean biogeochemistry, Science, 328 (2010) 1512–1516.

[2] H. Wang, X. Yuan, G. Zeng, L. Leng, X. Peng, K. Liao, L. Pengand, Z. Xiao, Removal of malachite green dye from wastewater by different organic acid-modified natural adsorbent: kinetics, equilibriums, mechanisms, practical application, and disposal of dye-loaded adsorbent, Environ. Sci. Pollut. Res. Int., 21 (2014) 11552–11564.

[3] I.A.W. Tan, A.L. Ahmad, B.H. Hameed, Adsorption of basic dye using activated carbon prepared from oil palm shell: batch and fixed-bed studies, Desalination, 225 (2008) 13–28.

[4] V.K. Gupta, Suhas, Application of low-cost adsorbents for dye removal – a review, J. Environ. Manage., 90 (2009) 2313–2342.

[5] A. Demirbas, Agricultural based activated carbons for the removal of dyes from aqueous solutions: a review, J. Hazard. Mater., 167 (2009) 1–9.

[6] Y. Liu, Y. Zheng, A. Wang, Enhanced adsorption of methylene blue from aqueous solution by chitosan-g-poly (acrylic acid)/ vermiculite hydro gel composites, J. Environ. Sci., 22 (2010) 486–493.

[7] M. Rafatullah, O. Sulaiman, R. Hashim, A. Ahmad, Adsorption of methylene blue on low-cost adsorbents: a review, J. Hazard. Mater., 177 (2010) 70–80.

[8] A.S. Franca, L.S. Oliveira, M.E. Ferreira, Kinetics and equilibrium studies of methylene blue adsorption by spent coffee grounds, Desalination, 249 (2009) 267–272.

[9] F. Deniz, S.D. Saygideger, Removal of a hazardous azo dye (Basic Red 46) from aqueous solution by princess tree leaf, Desalination, 268 (2011) 6–11.

[10] G.O. El-Sayed, Removal of methylene blue and crystal violet from aqueous solutions by palm kernel fiber, Desalination, 272 (2011) 225–232.

[11] A. Bhatnagar, A.K. Minocha, S.H. Kimand, B.H. Jeon, Removal of some metal ions from water using battery industry waste and its cement fixation, Fresenius Environ. Bull., 16 (2007) 1049–1055.

[12] S. Wang, Y. Boyjoo, A. Choueib, Z.H. Zhu, Removal of dyes from aqueous solution using fly ash and red mud, Water Res., 39 (2005) 129–138.

[13] S. Jain, R.V. Jayaram, Removal of basic dyes from aqueous solution by low cost adsorbent: wood apple shell (*Feronia acidissima*), Desalination, 250 (2010) 921–927.

[14] S. Wang, M. Wei, Y. Huang, Biosorption of multifold toxic heavy metal ions from aqueous water onto food residue eggshell membrane functionalized with ammonium thioglycolate, Agric. Food Chem., 61 (2013) 4988–4996.

[15] W. Wang, B. Chen, Y. Huang, J. Cao, Evaluation of eggshell membrane-based bioadsorbent for solid-phase extraction of linear alkylbenzene sulfonates coupled with high-performance liquid, J. Chromatogr., A, 1217 (2010) 5659.

[16] M. Baláz, Eggshell membrane biomaterial as a platform for applications in materials science, Acta Biomater., 10 (2014) 3827–3843.

[17] M. Arami, N.Y. Limaee, N.M. Mahmoodi, Evaluation of the adsorption kinetics and equilibrium for the potential removal of acid dyes using a biosorbent, Chem. Eng. J., 139 (2008) 2–10.

[18] N. Liu, Y. Liu, Y. Luan, X. Hu, The elimination of heavy metal-containing wastewater by eggshells membrane, Appl. Mech. Mater., 299 (2013) 207–210.

[19] Md. Tamez Uddin, Md. Rukanuzzaman, Md. Maksudur Rahman Khan, Md. Akhtarul Islam, Adsorption of methylene blue from aqueous solution by jackfruit (*Artocarpus heterophyllus*) leaf powder: a fixed-bed column study, J. Environ. Manage., 90 (2009) 3443–3450.

[20] R. Han, Y. Wang, W. Zou, Y. Wang, J. Shi, Comparison of linear and nonlinear analysis in estimating the Thomas model parameters for methylene blue adsorption onto natural zeolite in fixed-bed column, J. Hazard. Mater., 145 (2007) 331–335.

[21] V. Ponnusami, S. Vikram, S.N. Srivastava, Guava (*Psidium guajava*) leaf powder: novel adsorbent for removal of methylene blue from aqueous solutions, J. Hazard. Mater., 152 (2008) 276–286.

[22] S. Chen, Q. Yue, B. Gao, Q. Li, X. Xu, K. Fu, Adsorption of hexavalent chromium from aqueous solution by modified corn stalk: a fixed-bed column study, Bioresour. Technol., 113 (2012) 114–120.

[23] A.A. Ahmad, B.H. Hameed, Fixed-bed adsorption of reactive azo dye onto granular activated carbon prepared from waste, J. Hazard. Mater., 175 (2010) 298–303.

[24] R. Aravindhan, J.R. Rao, B.U. Nair, Preparation and characterization of activated carbon from marine macro-algal biomass, J. Hazard. Mater., 162 (2009) 688–694.

[25] M.C. de Hoces, G.B. Garcia, A.R. Galvez, M.A. Martin-Lara, Effect of the acid treatment of olive stone on the biosorption of lead in a packed-bed column, J. Ind. Eng. Chem. Res., 49 (2010) 12587–12595.

[26] G. Bohart, E.Q. Adams, Some aspects of the behaviour of charcoal with respect to chlorine, J. Am. Chem. Soc., 42 (1920) 523–544.

[27] A. Wolborska, Adsorption on activated carbon of *p*-nitrophenol from aqueous solution, Water Res., 23 (1989) 85–91.

[28] H.C. Thomas, Heterogeneous ion exchange in flowing system, J. Am. Chem. Soc., 66 (1944) 1664–1666.

[29] Y.H. Yoon, J.H. Nelson, Application of gas adsorption kinetics. I. A theoretical model for respirator cartridge service time, J. Am. Ind. Hyg. Assoc., 45 (1984) 509–516.

[30] J. Goel, K. Kadirvelu, C. Rajagopal, V.K. Garg, Removal of lead (II) by adsorption using treated granular activated carbon: batch and column studies, J. Hazard. Mater., 125 (2005) 211–220.

[31] T. Mathialagan, T. Viraraghavan, Adsorption of cadmium from aqueous solution by perlite, J. Hazard. Mater., 94 (2002) 291–303.

[32] I.A.W. Ta, B.H. Hameed, A.L, Ahmad, Equilibrium and kinetic, studies on basic dye adsorption by oil palm fiber activated carbon, Chem. Eng. J., 127 (2007) 111–119.

[33] D. Yang, L. Qi, J. Ma, Hierarchically ordered networks comprising crystalline ZrO_2 tubes through sol–gel mineralization of eggshell membranes, J. Mater. Chem., 13 (2003) 1119–1123.

[34] T. Weymuth, C.R. Jacob, M. Reiher, A local-mode model for understanding the dependence of the extended amide III vibrations on protein secondary structure, J. Phys. Chem., 114 (2010) 10649–10660.

[35] K.A. Whitehead, P.S. Benson, J. Verran, The detection of food soils on stainless steel using energy dispersive X-ray and Fourier transform infrared spectroscopy, Biofouling, 27 (2011) 907–917.

[36] D. Liu, Y.G. Li, H. Xu, S.Q. Sun, Z.T. Wang, Differentiation of the root of cultivated ginseng, mountain cultivated ginseng and mountain wild ginseng using FT-IR and two-dimensional correlation IR spectroscopy, J. Mol. Struct., 883 (2008) 228–235.

[37] S. Gunasekaran, E. Sailatha, Vibrational analysis of pyrazinamide, Ind. J. Pure Appl. Phys., 46 (2008) 315–320.

[38] A.P. Lim, A.Z. Aris, Continuous fixed-bed column study and adsorption modeling: removal of cadmium (II) and lead (II) ions in aqueous solution by dead calcareous skeletons, Biochem. Eng. J., 87 (2014) 50–61.

[39] L. Cavas, Z. Karabay, H. Alyuruk, H. Dogan, G.K. Demir, Thomas and artificial neural network models for the fixed-bed of methylene blue by a beach waste *Posidonia oceanica* (L.) dead leaves adsorption, Chem. Eng. J., 171 (2011) 557–562.

[40] E. Malkoc, Y. Nuhoglu, Fixed bed studies for the sorption of chromium (VI) onto tea factory waste, Chem. Eng. Sci., 61 (2006) 4363–4372.

[41] Z.Z. Chhowdhury, S.M. Zain, A.K. Rashid, R.F. Rafique, K. Khalid, Breakthrough curve analysis for column dynamics sorption of Mn(II) ions from wastewater by using *Mangostana garcinia* peel-based granular-activated carbon, J. Chem., 2013 (2013) 1–8.

[42] Z. Aksu, F. Gonen, Biosorption of phenol by immobilized activated sludge in a continuous packed bed: prediction of breakthrough curves, Process Biochem., 39 (2004) 599–613.

[43] R. Mazouz, N. Filali, Z. Hattab, K. Guerfi, Valorisation of granulated slag of Arcelor-Mettal (Algeria)in cationic dye adsorption from aquous solution: column studies, J. Water Reuse Desal., 4 (2016) 204–213.

[44] R. Han, Y. Wang, X. Zhao, Y. Wang, F. Xie, J. Cheng, M. Tang, Adsorption of methylene blue by phoenix tree leaf powder in a fixed bed column: experiments and prediction of breakthrough curves, Desalination, 245 (2009) 284–297.
[45] W. Zhang, L. Dong, H. Yan, H. Li, Z. Jiang, X. Kan, H. Yang, A. Li, R. Cheng, Removal of methylene blue from aqueous solutions by straw based adsorbent in a fixed bed column, Chem. Eng. J., 173 (2011) 429–436.
[46] B. Koumanova, P. Peeva, S.J. Allen, K.A. Gallagher, M.G. Healy, Biosorption from aqueous solutions by eggshell membranes and *Rhizopus oryzae*: equilibrium and kinetic studies, Chem. Technol. Biotechnol., 77 (2002) 539–545.
[47] F. Momenbeik, F. Tajmir Riahi, Chemically modified eggshell membrane as an adsorbent for solid-phase extraction of morphine followed by high performance liquid chromatography analysis, Anal. Bioanal. Chem. Res., 1 (2014) 108–116.
[48] M. Auta, B.H. Hameed, Chitosan–clay composite as highly effective and low-cost adsorbent for batch and fixed-bed adsorption of methylene blue, Chem. Eng. J., 237 (2014) 352–361.
[49] S.S. Baral, S.N. Das, P. Rath, Hexavalent chromium removal from aqueous solution by adsorption on treated sawdust, Biochem. Eng. J., 31 (2006) 216–222.
[50] F.G. Torres, O.P. Troncoso, M.R. Montes, The effect of temperature on the mechanical properties of a protein-based biopolymer network the eggshell membrane, J. Therm. Anal. Calorim., 11 (2013) 1921–1925.
[51] M.J. Jaycock, G.D. Parfitt, Chemistry of Interfaces, Ellis Horwood Ltd., Chichester, 1981.
[52] N. Ozturk, D. Kavak, Adsorption of boron from aqueous solutions using fly ash: batch and column studies, J. Hazard. Mater., B127 (2005) 81–88.
[53] E.K. Guechi, O. Hamdaoui, Evaluation of potato peel as a novel adsorbent for the removal of Cu(II) from aqueous solutions: equilibrium, kinetic, and thermodynamic studies., Desal, Wat. Treat., 57 (2016) 10677–10688.
[54] C. Djelloul, O. Hamdaoui, Removal of cationic dye from aqueous solution using melon peel as non conventional low-cost sorbent, Desal. Wat. Treat., 52 (2014) 7701–7710.
[55] S. Nawaz, H.N. Bhatti, T.H. Bokhari, S. Sadaf, Removal of novacron golden yellow dye from aqueous solutions by low-cost agricultural waste: batch and fixed bed study, Chem. Ecol., 30 (2014) 52–65.
[56] F. Banat, S. Al-Asheh, R. Al-Ahmad, F. Bni-Khalid, Bench-scale and packed bed sorption of methylene blue using treated olive pomace and charcoal, Bioresour. Technol., 98 (2007) 3017–3025.
[57] D.D. Salman, W.S. Ulaiwi, N.M. Tariq, Determination the optimal conditions of Methylene Blue, Int. J. Poult. Sci., 11 (2012) 391–396.